Author version: *Estuar. Coast. Shelf Sci., vol.134; 2013; 1-10*

Sub-tidal water-level oscillations in the Mandovi estuary, west coast of India

S.R. Shetye [a]* and V. Vijith [b]

[a] Goa University, Taleigao, Goa 403206, India

[b] CSIR – National Institute of Oceanography, Dona Paula, Goa, 403004, India

* Corresponding author

E-mail: *shetye@unigoa.ac.in* ; Telephone number: +91 9011056605

Abstract.

Using water-level data collected at six locations during March – April 2003 in the main channel of the Mandovi estuary, one of the 50 odd estuaries on the west coast of India, we describe the nature of variability of water level in the estuary at periods longer than two days. We then examine the causes behind the variability using data on wind and current measured near the mouth of the estuary. The main channel of the estuary is 50 km long and March – April is a period when local winds are weak. Our analysis shows that an important factor that generates sea-level variability at the mouth of the estuary is the northward propagating coastal-trapped waves, which are frequently observed along the coast and have sea-level variations that are in approximate geostrophic equilibrium. We also raise the possibility that local winds generate currents and associated sea-level variations. The relationship between the wind, the current and the sea level in this case, which is expected to be ageostrophic, needs further study. Once generated, a sea-level oscillation at the mouth propagates into the estuary undamped. Geometric amplification arising from convergence of the estuarine channel from mouth to head balances frictional dissipation to sustain the undamped propagation.

Keywords: sub-tidal; oscillations; propagation; estuaries; geostrophy; India

1. Introduction

The North Indian Ocean, i.e., the part of the Indian Ocean that lies to the north of about 10^{o}S, is a tropical basin that is restricted to the south of about 25^{o}N by the Asian subcontinent. The tropical basins of the Atlantic and the Pacific are known for the steady surface winds that they experience throughout the year in the form of the trade winds that blow from the northeast (southeast) in the northern (southern) hemisphere. Unlike the surface winds over these basins, the magnitude and direction of surface winds over the North Indian Ocean show a distinct annual cycle. The overall direction of the winds north of the equator during May – October is southwesterly. This season is referred to as the southwest or summer monsoon. The winds are northeasterly during November – February, the northeast or winter monsoon. The winds are significantly stronger during the summer monsoon. The times of transition from one monsoon to the other are times of weak winds. Superimposed on the seasonal cycle of winds are variations with periods from a few days to a few months, including biweekly (once every two weeks) oscillations (Krishnamurti and Bhalme, 1976) and Madden-Julian oscillations (Madden and Julian, 1971, 1972).

The monsoon winds and the winds with other periodicities drive currents with the same periodicities in the basin. The most important mechanism for the driving is the generation of equatorially- and coastal-trapped waves. The North Indian Ocean is small in comparison to the north and south Atlantic and Pacific, primarily because its meridional stretch from the equator is small, only about 2,800 km; the meridional stretch of the Pacific and Atlantic is in excess of 7,000 km. The smaller size of the North Indian Ocean ensures that the equatorially- and coastal-trapped waves play a major role in determining the nature of circulation over the ocean in the coastal as well as in the open sea (McCreary et al., 1993; and Shankar et al., 2002).

Preferred position of Figure 1

The de-tided sea level along the coast of India shows the presence of intraseasonal to interannual oscillations. This can be seen from Figure 1, which shows de-tided and 2-day low-passed sea level at 6 locations along the coast of India. Three of these stations, Paradip, Visakhapatnam and Chennai, are on the east coast; the remaining stations, Kochi, Mormugao and Okha, are on the west coast (see inset of Figure 2). The sea level shown in the figure reveals variability at a wide spectrum of periods ranging

from days to interannual time scales. Durand et al. (2009) have examined variability of the current along the east coast of India, the East India Coastal Current, on some of these time scales using altimeter data. More recently, Amol et al. (2012) used data from six Acoustic Doppler Current Profiler (ADCP) moorings deployed during March – September 2008 on the continental shelf and slope off the central west coast of India to present evidence for poleward propagation of shelf or coastal-trapped waves (CTWs). They reported wave propagation on the shelf in the 20–40-day, 10–14-day, and 3–5-day-period bands and noted that remote forcing was important even at periods as short as 4 days and even when the local along-shore wind is strong. The authors further noted that remotely-forced waves are particularly prominent when the local winds are weak, as during March – April.

The east and the west coast of India are dotted with about a hundred estuaries that have some special features due to another aspect of the monsoons, the precipitation. About 80% of the rainfall received by the Indian subcontinent falls during the summer monsoon, often referred to as the Indian Summer Monsoon (ISM). Gadgil (2003) provides an overview of the pattern of rainfall associated with the ISM and its interannual and intraseasonal variability. With most of the rainfall occurring during the wet ISM, most of the runoff into the estuaries is also during the same season. There is virtually no runoff into the estuaries after some time following the withdrawal of the ISM. This feature gives the estuaries special characteristics that have led to naming them as monsoonal estuaries. Vijith et al. (2009) and Vijith and Shetye (2012) have discussed their special characteristics.

What is the nature of variability of the de-tided water level in a monsoonal estuary during the dry season? Do the variations seen in de-tided sea level along a stretch of the coast of India due to passage of CTWs have an impact on the de-tided water level within an estuary that opens to the sea at a point along the stretch? If yes, what is the mechanism for propagation of coastal sea-level variability into the estuarine channel? In this paper, we address these questions by first using data on water level collected for a month during March – April 2003 in the Mandovi estuary in Goa, central west coast of India; and second, by using an analytical model for propagation of surface waves into an estuary. The Mandovi estuary is well suited for this study for two reasons. First, remotely- and locally-driven CTWs along the coast of Goa during March – April 2003 have been studied earlier by Shetye et al. (2008). Hence, some understanding exists about the nature and the causes of the coastal sea-level variability at the time when the water level was measured within the Mandovi estuary. Second, the Mandovi is amongst the best

studied estuaries of India; Sundar and Shetye (2005) have described the nature of tides in the estuary; Shetye et al. (2007) provide an overview of the physics, chemistry, and biology; and Vijith et al. (2009) have described the annual cycle of salinity and runoff into the estuary. The study of Vijith et al. (2009) and Vijith and Shetye (2012) examine distinguishing features of stratification in the estuary, primarily arising from the nature of runoff into the estuary, that justifies it to being called a *monsoonal estuary*.

In the next section, we discuss the geographic setting of the Mandovi and Zuari estuaries in the state of Goa on the west coast of India. Section 3 describes the data that were collected during March-April 2003, their analysis, and the main features revealed by the analysis. Section 4 summarizes the propagation of sub-tidal water-level oscillations in the Mandovi. The conclusions are summarized in Section 5. In Appendix A, we use an analytical model to put the observed features in perspective.

2. Geometry of the Mandovi estuary

The Mandovi is widest in the Aguada Bay, the width here being approximately 4 km. The bay is 4 km long, and is, on average, marginally deeper than the rest of the estuarine channel, the average depth in the bay being about 5 m. As seen in Figure 2, a number of rivers join the Mandovi. The 30 km stretch of the main channel of the Mandovi gets progressively narrower and shallower in the upstream direction. At the upstream end of the Mandovi, near Ganjem, lies the Mhadei River, the major supplier of runoff to the Mandovi during the monsoon. A smaller river, Ragda, also joins the Mandovi near Ganjem.

Preferred position of Figures 2 and 3

The depth of the main channels of the Mandovi varies considerably with location. This is brought out in Figure 3, which shows the variation of the depth along a line in the middle of the main channel of the Mandovi. The cross-sectional area of the channel of the estuary drops in the upstream direction (Figure 3). The drop is most rapid near the mouth but continues farther upstream too. The drop is primarily due to the decrease in channel width. Such channels have often been described as ‘strongly-convergent’ (Friedrichs and Aubrey, 1994). The convergence has important implications for the dynamics of gravity waves, including tides, in the estuarine channels. The Mandovi estuary is joined by a narrow canal, the Cumbarjua Canal, that connects it to another estuary, the Zuari (see Figure 2). The cross-sectional area of the canal is, however, much too small to have a major impact on the dynamics in the two main channels.

3. Data and analysis

The data used here are a part of a dataset that includes water-level variation within the estuary, winds measured at a location near the mouth of the estuary and currents measured at five locations in the vicinity of the coast of Goa. The data were collected for a month during March – April 2003 under a program on Integrated Coastal and Marine Area Management (ICMAM) conducted by the National Institute of Oceanography, Goa. Some of the data have been used earlier in Shetye et al. (2008) to discuss the dynamics of along-shore current in the region. They, however, did not discuss the data within the estuary, nor the underlying dynamics behind the variability observed in the estuary.

Wind speed and direction were measured at every 10 minutes using an automatic weather station located on the terrace of the National Institute of Oceanography (see Figure 2 for location) during 10 March to 14 April 2003. Prominent in the wind record is the sea breeze, as seen in typical (Aparna et al., 2005) and average (Neetu et al., 2006) hodographs for the period. Aparna et al., 2005, also showed that the anemometer winds are significantly correlated with the winds measured by the QuikSCAT scatterometer; the QuikSCAT winds are estimated at the standard height of 10 m.

During 18 March to 17 April 2003 currents were measured at five locations along the coast of Goa and have been discussed in detail in Shetye et al. (2008). The currents were measured using Aanderaa self-recording current meters, each of which was located at mid-depth in the water column. The water column depths at the locations of deployment of the current meters varied between 10 m to 48 m. The currents were measured at an interval of 10 minutes. The zonal and meridional components of the currents were first de-tided using the software Tidal Analysis Software Kit (TASK; Bell et al., 1998). The de-tided (residual) current components were then rotated to yield the along-shore and cross-shore components. The rotation angle was estimated by minimizing the cross-shore component in the least squares sense: the assumption here was that the non-tidal component of the current would be largely along-shore. The along-shore components of the residual at the five locations were visually coherent (see Figure 2 in Shetye et al., 2008), implying a common forcing mechanism. The cross correlations of the along-shore components were also significant at the 99% level (Table 2 in Shetye et al., 2008). Later on in this section, we have analyzed data from one of the five current meters, the one located near the mouth of the estuary. The location of this current meter is shown in Figure 2.

Water levels in the main channel of the Mandovi at the locations shown in Figure 2 were measured using tide poles manned continuously by tide-pole observers. Data were recorded once every 15 minutes at the 6 locations shown in Figure 2. The zero of each tide-pole used in the observations was referenced to a 'local chart datum' for future reference. The tide-pole readers worked in three shifts during a day. Each reader was requested to visually average the water level for about a minute and then record the average water level. The 15-minute data were analyzed using TASK to determine tidal amplitude and phase lag of 26 major constituents and 8 related constituents. The analysis served as a tool for quality control too. Data points with large residuals were examined to determine if the residuals were due to errors in recording. If inferred to be so, the suspect data were removed. The total number of points removed in a time-series was highest, (2.6 % or 87 points from a total of 3360) at Usgao (see Figure 2; location 5). The number of points removed at each of the rest of the stations was less than 1%. All computations were referenced to the Indian Standard Time, which leads the UTC by 330 minutes.

The water-level data used here have been used earlier by Sundar and Shetye (2005) to describe tides within the Mandovi and Zuari estuaries. It is not clear what the error associated with tide-pole measurement is. Sundar and Shetye (2005) did attempt to quantify this with reference to their estimates of tidal constituents and concluded that for all constituents whose amplitude is greater than 3 cm, the upper limit of the error bar is ±0.5 cm for amplitude and ±5 degree for phase lag.

Preferred position of Figures 4 and 5

The quality-controlled data at the above 6 locations are shown in Figure 4. Figure 5 shows the residual water level, i.e., the water level after subtracting the water level associated with the tide from the data shown in Figure 4. While there is considerable scatter, mainly arising from oscillations with period of a day or so, oscillations with longer periods are discernible in the data at all stations. To highlight these lower frequency oscillations, the data were filtered with a third-order Butterworth low-pass filter with a cut-off frequency of 0.5 per day to remove the high-frequency noise. The two-day low-passed de-tided water levels are shown by the black curves in Figure 5. In order to apply the filter, it was necessary to fill the missing residual values that were removed as a part of the quality control of data. The missing values in the time-series of residual values were filled by using linear interpolation between the residual value before a gap and that after a gap.

Deployed at Verem, near the mouth of the Mandovi, was a Valeport pressure-sensor tide gauge in addition to the tide-pole. Shown in the panel at the bottom of Figure 5 is the residual water level computed using the automated tide gauge at Verem. The tide gauge data were not corrected for barometric pressure variation. Comparison of the residual water level computed using the pressure sensor versus that using the tide pole shows that the high-frequency scatter is larger for the tide-pole measurements. However, the low-pass filtered variability is virtually identical in the tide-pole and Valeport data. The correlation between the two is 0.86. To compute the correlation the Valeport observations were sub-sampled to the times of the tide-pole observations using cubical interpolation. This was required because the tide-pole observations were at every 15 minutes interval, whereas Valeport observations were at 10 minutes. The fact that the variability seen in the de-tided filtered data in tide-pole data is virtually identical to that seen in automated data at Verem suggests that the quality of tide-pole data is good enough for this study.

Preferred position of Figure 6

Sundar and Shetye (2005) in their analysis of the tides in the Mandovi and Zuari estuaries have noted that the stations at the upstream ends of the two channels experienced obstruction to tidal flow due to the higher elevation of these two stations. The tidal flow could reach here only when the water level was higher than a threshold. In view of the obstruction to the flow due to the increase in elevation, we have ignored data from Ganjem, the station farthest from the mouth of the Mandovi. We will therefore restrict the rest of the analysis to the following five stations: Verem, Britona, Akkada, Volvoi and Usgao (see Figure 5).

A wavelet analysis of the data from these stations is shown in Figure 6. A feature that stands out for each of the stations shown in this figure is a band of water-level oscillations with periods centered around 5 days during the second half of March 2003. The amplitude of the oscillation remained unchanged at the 5 stations. The observed feature raises two questions. First, what were the causes behind the water-level oscillations seen at the mouth of the estuary? Second, once an oscillation is produced at the mouth, how does it propagate into the estuarine channel? We address the first question in the remainder of this section. The second is examined in the next section.

Preferred position of Figures 7 and 8

We assume that the oscillations at the mouth are caused by dynamics of the current on the shelf off the estuarine mouth. Two mechanisms for generating sea-level oscillations at the coast are: geostrophic adjustment of a remotely forced current; and oscillations forced by local winds that could be ageostrophic.

Figure 7 shows a wavelet analysis of the along-shore current measured at the mouth of the Mandovi and Zuari (see Figure 2 for location of the current meter). A feature similar to that seen in the wavelet analysis of water level shown in Figure 6, i.e., oscillations with periods centered around 5 days during the second half of March 2003, is also seen in the wavelet analysis of the along-shore current.

Wavelet analysis of winds measured near the mouth of the Mandovi and Zuari estuaries (see Figure 2 for location of the anemometer used to measure winds) is shown in Figure 8. From the figure, we note that during the second half of March 2003 the winds did not have oscillations whose characteristics match with those of water level (Figure 6) and of the along-shore current (Figure 7). Hence the feature seen in the water level and the current must have resulted from remote forcing.

Shetye et al. (2008) have noted that the sea level at the mouth of the estuary, i.e., at Verem, was significantly correlated with the along-shore current measured at the mouth of the Mandovi and Zuari estuaries and with the along-shore currents measured to the north and to the south of the mouth (see their Table 2). Correlation between the water level at Verem and the along-shore current at the mouth of Mandovi and Zuari was 0.71, which is significant at the 99% confidence level, with the water level lagging the current by almost a day: 23 hours 20 minutes. This suggests that at least an approximate geostrophic balance must have held for the along-shore current with sea level dropping (rising) at the coast whenever there was a southward (northward) current.

Preferred position of Figure 9

To examine this balance we computed the along-shore geostrophic current (v) by using the geostrophic relation,

$$v = \frac{g}{f}\frac{\partial \eta}{\partial x} \approx \frac{g\eta}{fL}; \qquad (1)$$

where g is the acceleration due to gravity, η is the de-tided sea level at the coast and f is the Coriolis parameter. We take f to be $3.9\times10^{-5}s^{-1}$, appropriate for the latitude 15.5°N and g to be $9.8ms^{-2}$. The de-tided 2-day low-passed sea level measured at Verem is used as η. L is the distance from the coast to a point on the shelf up to which the sea-level slope is assumed to occur. We took this distance to be 126 km. The velocity computed using the above expression was then advanced by 23 hours and 20 minutes, which was done to compensate for the observed lag of sea level behind the along-shore current. The velocity thus computed and the observed along-shore current are shown in Figure 9. The good match between the two and the high correlation noted earlier show that geostrophy is indeed a good approximation to the dynamics of the current along the coast. We chose L to be 126 km by trial and error to minimize the sum of the squares of deviation between the two curves shown in Figure 9. We note that the width of the shelf off Goa, estimated as the distance from the coast to the 200 m isobath, is about 110 km.

Along-shore current in approximate geostrophic balance with sea level at the coast either leading or lagging the current has been noticed along many coasts that have CTWs propagating along them (see for example, Schwing et al., 1983). Figure 9 is therefore in support of the inference drawn by Amol et al. (2012) and earlier by Shetye et al. (2008) that remotely forced CTWs are an important factor in the dynamics underlying the along-shore current and sea-level variability on the coast. Hence, sea-level variability arising from approximate geostrophic balance in the CTWs propagating along the coast is important at the mouth of the Mandovi. We expect the same to hold true for other estuaries with similar geometry on the west coast of India.

While there are similarities between the two curves shown in Figure 9, there are also differences. A likely cause for the differences is the local wind, which may set up a current that may be ageostrophic. A noteworthy feature in the wavelet analysis of along-shore wind stress shown in Figure 8 is an oscillation with periods between 5 and 10 days during the first two weeks of April 2003. This feature does have a match with the analysis of along-shore current shown in Figure 7. However, no similar match can be seen in the analysis of water level in Figure 6. The match between wind and along-shore

current analyses and the absence of a match between wind and water-level analysis raises the possibility that the along-shore winds did generate a locally-forced current, but it was ageostrophic. This possibility, i.e. contribution to sub-tidal sea-level variability due to local winds along this coast, needs to be examined further. Here we are raising it as a general possibility. We expect the relationship between sea level, wind and current in this case to be ageostrophic and more complicated than that associated with geostrophy. We note here that Shetye et al. (2008) concluded that the high-passed (i.e. with periods less than 10 days) component of along-shore current was strongly correlated (correlation coefficient 0.6-0.7) with high-passed component of the along-shore wind, the current lagging the wind by half a day. We expect the contribution of the local wind to the sea-level variability to be higher at the times of stronger winds such as the summer monsoon.

4. Propagation into the estuary

Once a water-level oscillation is set up at the mouth of an estuary, how does the oscillation propagate into the estuarine channel? In particular, how is amplitude of the oscillation affected (see Figures 5 and 6) as a disturbance propagates through the channel? We address these questions in Appendix A using an analytical model that assumes that the dynamics underlying sub-tidal oscillations in the Mandovi estuary are the same as the dynamics of tidal propagation in such estuaries. The Mandovi, like many other channels found along the west coast of India, is narrow and shallow, and has a channel that converges, i.e., its cross-sectional area reduces from mouth to head. As noted in the Appendix, because of the convergence, frictional dissipation is balanced by geometric amplification to preserve the amplitude of an oscillation as it propagates from mouth to head. Similar behaviour with regard to tides in the Mandovi has been discussed earlier in Unnikrishnan et al. (1997) and Shetye (1999). Figure 6 shows that the same behaviour is seen in the case of the oscillations at sub-tidal frequencies.

5. Concluding comments

In the present study we have described the variability of water level seen in the Mandovi during a month in March – April 2003 and have analysed the causes behind the observed features of the variability. We show that the passage of a CTW is an important mechanism that generates sea-level variability at the mouth of the estuary. Whenever remotely forced CTWs, which are ubiquitous along the west coast of India, pass by the mouth of the estuary, they generate sea-level oscillations consistent with the periods

and amplitudes of the waves. This sea-level variability is in approximate geostrophic balance. We also raise the possibility that local wind drives a current and associated sea-level variation. The relationship between the wind, the current and the sea level in this case is expected to be ageostrophic and more complex than that seen in the case of geostrophic equilibrium. This relationship needs further study.

The sea-level oscillations caused at the mouth of the estuary by the above two mechanisms propagate into the estuary as undamped surface gravity waves. The undamped propagation is possible because frictional dissipation of the waves is balanced by amplification due to geometric confinement arising from the convergent nature of the estuarine channel.

The present study is based on month-long observations during March – April, which is known to be a time of weak winds along the coast. Amol et al. (2012) have noted that CTWs are ubiquitous along the coast and that they persist even during periods of strong winds, such as the summer monsoon, i.e. the ISM. Hence the first cause listed above should apply throughout the year. Contribution of the second depends on the strength of local winds. During, ISM, when local winds are strongest, the second is expected to play a much larger role. However, another factor which is not discussed here needs to be considered during this time, which is a time of rainfall over the Indian Peninsula. The central west coast of India being a region of high precipitation, the runoff in the Mandovi is high and strongly time-dependent (Vijith et al., 2009) during the ISM. The water-level variation associated with the variation in runoff is expected to dominate in the estuarine channel during the ISM.

The role of CTWs in generating sea-level variability at the mouth of the estuary implies that two widely separated estuaries along the coast could experience similar variability due to the passage of a group of CTWs along the coast. In essence, the estuaries can experience teleconnections. This possibility needs to be checked empirically.

Acknowledgements

We acknowledge Suprit Kumar, Amol Prakash and D. Shankar for their help during this study. Critical comments from two anonymous reviewers helped to improve the manuscript. V. Vijith acknowledges the CSIR for his research fellowship. The FORTRAN code for wavelet analysis was downloaded from http://paos.colorado.edu/research/wavelets. All figures in this paper are made using Generic Mapping Tools. This is NIO contribution XXXX.

Appendix A

Consider an estuarine channel that is typical of the channels found along the west coast of India, including the Mandovi: narrow and shallow with converging channels. We assume the dynamics underlying propagating sub-tidal oscillations in the channels to be the same as that in the case of tidal flows. Ignoring the wind stress, the equations governing continuity and momentum balance in such a case can be approximated by, respectively (see, for example, Equations 3.2 and 3.3, in Friedrichs, 2010),

$$b\frac{\partial \eta}{\partial t} = -\frac{\partial}{\partial x}(ubh) \qquad \text{(A1)}$$

and

$$\frac{\partial u}{\partial t} + u\frac{\partial u}{\partial x} + g\frac{\partial \eta}{\partial x} = \frac{\tau_b}{\rho h_0}, \qquad \text{(A2)}$$

where x is the co-ordinate in the upstream direction and t is time; η and u are perturbations of the surface elevation and upstream velocity, respectively; h is the depth of the channel and b is its width; ρ is the density (assumed to be constant) and τ_b is the bottom stress.

We now make the following approximations. First, width b varies as $B_0 e^{-x/L_b}$, i.e., the convergent channel has width that decreases exponentially with distance x in the upstream direction; B_0 is a constant. Second, depth, h, remains constant and equals h_0. Third, perturbation of the surface elevation is much smaller than the channel depth, i.e. $\eta << h_0$. Fourth, the bottom stress term on the right hand side of the momentum equation can be approximated as $\frac{\tau_b}{\rho h_0} = -ru$, where r is a constant. Finally, numerical models for the Mandovi and Zuari estuaries have shown that, like other shallow estuaries, the momentum balance is primarily between friction and pressure gradient (Unnikrishan et al., 1997). Therefore, we simplify the momentum equation (A2) to include only these two terms.

With these approximations the equations for continuity and momentum become,

$$\frac{\partial \eta}{\partial t} = -h_0 \frac{\partial u}{\partial x} + \frac{h_0}{L_b} u \qquad \text{(A3)}$$

and

$$g \frac{\partial \eta}{\partial x} = -ru\,. \qquad \text{(A4)}$$

The two equations lead to the following single equation for η (see Shetye, 1999),

$$\frac{\partial \eta}{\partial t} - \frac{c_0^2}{r} \frac{\partial^2 \eta}{\partial x^2} + \frac{c_0^2}{r L_b} \frac{\partial \eta}{\partial x} = 0\,, \qquad \text{(A5)}$$

where, $c_0^2 = gh$. The equations permit waves with frequency ω and wave number k, where

$$k_{1,2} = \frac{1}{2\mathrm{L}_b} \left[-i \pm i \sqrt{1 - i \frac{4\mathrm{L}_b^2 \omega r}{c_0^2}} \right]. \qquad \text{(A6)}$$

Suitable values for the variables in the above equation for the Mandovi estuary, which is about 50 km long, are: L_b =7.5 km; r =10^{-3} s^{-1}; h_0 is estimated to be 2 – 5 m. Taking $\omega = \frac{2\pi}{24 \times 3600 \times T_d}$ where T_d is the wave period in days, we get

$$k_{1,2} = \frac{1}{2\mathrm{L}_b} \left[-i \pm i \sqrt{1 - i\alpha} \right], \text{ where } \alpha = \left(\frac{4\mathrm{L}_b^2 r}{c_0^2} \frac{2\pi}{24 \times 3600 \times T_d} \right). \qquad \text{(A7)}$$

Preferred position of Table A1

Table A1 below gives the values of wavelengths (which depend on the real part of the wave number) and decay-lengths (dependent on the imaginary parts) for parameters suitable to the Mandovi and g=9.8 m s^{-2}. Note that the reflected wave always decays as it propagates downstream. This is because both friction and geometric effect (movement towards wider area) have damping effects on this wave. The e-folding decay length of this wave is of the same order as the e-folding convergence length of the estuary (taken to be 7.5 km for Mandovi). For periods up to about half a day, the wavelengths of the incident wave, reflected wave, and e-folding amplification length of the incident wave are all of the same order and increase with wave period.

As the period increases, α decreases, with the following implications to the incident and reflected waves. The e-folding length for amplification of the incident wave increases. For a period of a day, the e-folding length becomes much larger than the length of the estuary. In essence, the estuarine channel does not experience any appreciable increase from mouth to head. Simultaneously, the e-folding length of the reflected wave becomes much smaller than the length of the estuary. This implies that the reflected wave becomes irrelevant because it decays rapidly. There is empirical evidence to support this behavior. The amplitude of M2 increases by about 20% in the Mandovi, but the increase is less than 10% for K1. As the period increases to more than a day, this tendency, i.e., the incident wave's propagation with the same amplitude and the reflected wave's irrelevance increases. A useful approximation for periods of the order of a day and longer, i.e., for small α, is to drop the term $h_0 \frac{\partial u}{\partial x}$ in the continuity equation. This leads to a first-order governing equation for the waves in the channel leading to existence of only an un-damped incident wave. Amplification or decay of the wave is ruled out because frictional tendency to decay is exactly balanced by geometric tendency to amplify, as noted by Friedrichs and Aubrey (1994). With the approximation, the continuity and momentum equations become

$$\frac{\partial \eta}{\partial t} = \frac{h_0}{L_b} u \qquad \text{(A8)}$$

and

$$g \frac{\partial \eta}{\partial x} = -ru \,. \qquad \text{(A9)}$$

The two equations can be combined into $\frac{\partial \eta}{\partial t} + \frac{g h_0}{r L_b} \frac{\partial \eta}{\partial x} = 0$. (A10)

The solution, with the boundary condition that $\eta = \eta_0 e^{-i\omega t}$ at $x = 0$, is

$$\eta = \eta_0 e^{i\left(\frac{L_b \omega r}{g h_0} x - \omega t\right)} \,. \qquad \text{(A11)}$$

This is a free wave that propagates with the phase velocity $\left(\frac{g h_0}{L_b r}\right)$, which is about 4 m s^{-1} if the depth is taken to be 3 m.

References

Amol, P., Shankar, D., Aparna, S.G., Shenoi, S.S.C., Fernando, V., Shetye, S.R., Mukherjee, A., Agarvadekar, Y., Khalap, S., Satelkar, N.P., 2012. Observational evidence from direct current measurements for propagation of remotely forced waves on the shelf off the west coast of India. Journal of Geophysical Research 117, C05017, 15 pp, doi:10.1029/2011JC007606.

Aparna, M., Shetye, S.R., Shankar,D., Shenoi, S. S. C., Mehra, P., Desai, R.G.P., 2005. Estimating the seaward extent of sea breeze from QuikSCAT scatterometry. Geophysical Research Letters 32, L13601, doi:10.1029/2005GL023107.

Bell, C., Vassie, J. M., Woodworth, P. L., 1998. POL-PSMSL Tidal Analysis Software Kit 2000 (TASK-2000), Permanent Service for Mean Sea Level, Proudman Oceanographic Laboratory, Merseyside, U.K.

Durand, F., Shankar, D., Birol, F., Shenoi, S. S. C., 2009. Spatiotemporal structure of the East India Coastal Current from satellite altimetry. Journal of Geophysical Research 114, C02013, doi:10.1029/2008JC004807.

Emery, W. J., Thomson, R.E., 2001. Chapter 5 - Time-series Analysis Methods, Data Analysis Methods in Physical Oceanography, Elsevier Science, Amsterdam, 2001, Pages 371-567.

Friedrichs, C.T., Aubrey, D.G., 1994. Tidal propagation in strongly convergent channels. Journal of Gephysical Research 99, 3321-3336.

Friedrichs, C.T., 2010. Barotropic tides in channelized estuaries. In: Valle-Levinson, A. (Ed.), Contemporary issues in estuarine physics, Cambridge University Press, Cambridge, pp 27-61.

Gadgil, S., 2003. The Indian monsoon and its variability. Annual Review of Earth and Planetary Sciences 31, 429-467.

Krishnamurti, T. N., Bhalme, H.N., 1976. Oscillations of a monsoon system. Part I. Observational aspect. Journal of the Atmospheric Sciences 33, 1937 – 1954.

Madden, R. A., Julian, P.R., 1971. Description of a 40 – 50 day oscillation in the zonal wind in the tropical Pacific. Journal of the Atmospheric Sciences 28, 702 – 708.

Madden, R. A., Julian, P.R., 1972. Description of global-scale circulation cells in the tropics with a 40 – 50 day period. Journal of the Atmospheric Sciences 29, 1109 – 1123.

McCreary, J. P., Kundu, P.K., Molinari, R.L., 1993. A numerical investigation of the dynamics, thermodynamics and mixed-layer processes in the Indian Ocean. Progress in Oceanography 31, 181 – 244.

Neetu, S., Shetye, S.R., Chandramohan, P., 2006. Impact of sea breeze on wind-seas off Goa, west coast of India. Journal of Earth System Science 115, 229 – 234.

Schwing, F.B., Kjerfve, B., Sneed, J.E., 1983. Nearshore coastal currents on the South Carolina continental shelf. Journal of Geophysical Research 88 (C8), 4719-4729.

Shankar, D., Vinayachandran, P.N., Unnikrishnan, A.S., 2002. The monsoon currents in the north Indian Ocean. Progress in Oceanography 52, 63 – 120.

Shetye, S.R., 1999. Propagation of tides in the Mandovi and Zuari estuaries. Sadhana 24(1-2), 5-16.

Shetye, S.R., Dileep Kumar, M., Shankar, D., (Ed.), 2007. The Mandovi and Zuari estuaries. National Institute of Oceanography, Goa, India, 145 pp, available at http://drs.nio.org/drs/handle/2264/1032.

Shetye, S. R., Suresh, I., Shankar, D., Sundar, D., Jayakumar, S., Mehra, P., Prabhudesai, R.G., Pednekar, P.S., 2008. Observational evidence for remote forcing of the West India Coastal Current. Journal of Geophysical Research 113, C11001, doi:10.1029/2008JC004874.

Sundar, D., Shetye, S.R., 2005. Tides in the Mandovi and Zuari estuaries, Goa, west coast of India. Journal of Earth System Science 114 (5), 493-503.

Torrence, C., Compo, G.P., 1998. A Practical Guide to Wavelet Analysis. Bulletin of the American Meteorological Society 79, 61-78.

Unnikrishnan, A.S., Shetye, S.R., Gouveia, A.D., 1997. Tidal propagation in the Mandovi-Zuari Estuarine network, west coast of India: Impact of freshwater influx. Estuarine, Coastal and Shelf Science 45(6), 737-744.

Vijith, V., Shetye, S.R., 2012. A stratification prediction diagram from characteristics of geometry, tides and runoff for estuaries with a prominent channel. Estuarine, Coastal and Shelf Science 98, 101-107.

Vijith, V., Sundar, D., Shetye, S.R., 2009. Time-dependence of salinity in monsoonal estuaries. Estuarine, Coastal and Shelf Science 85, 601-608.

Figure captions

Figure 1: De-tided and 2-day low-passed hourly sea level (cm) during 2005 – 2006 at Paradip, Visakhapatnam, Chennai (Madras), Kochi (Cochin), Mormugao in Goa, and Okha; see the inset of Figure 2 for locations. The de-tiding was done using the software, Tidal Analysis Software Kit (TASK; Bell et al., 1998). Tidal constituents with periods of 28 hours and less were removed to de-tide the data. 2-day low-pass filter was applied after de-tiding. Day 1 is 1 January 2005. The solid line in each frame separates 2005 from 2006. Gaps are due to missing data. The sea-level data used in this figure are from tide gauges maintained by the Survey of India, archived at the Indian National Centre for Ocean Information Services (INCOIS), Hyderabad, India (www.incois.gov.in).

Figure 2: Map of the Mandovi and Zuari estuaries based on publications from the Survey of India (1967), the Naval Hydrographic Office, India, and the Admiralty, U.K. The depth contours (m) are with respect to mean sea level which is 1.3 m above Spring Low Water at Mormugao, which is a port located near the mouth of Zuari. To avoid clutter, the depth contours are shown only near the mouths of the Mandovi and the Zuari. "T" in a circle shows location up to which tidal influence is felt in the rivers Kushavati, Uguem, Guloli, Khandepar, and Mandovi. Land elevation is shown in colour, the scale for which is given above the figure. The locations where water-level observations were carried out are marked with a number in a circle. The name of the location can be determined by the number in the circle: (1) Verem; (2) Britona; (3) Akkada; (4) Valpoi; (5) Usgao; (6) Ganjem. "C" in a circle denotes the location of the current meter. "A" in a circle marks the location of the Automated Weather Station where winds used in the study were measured. The inset shows locations: Paradip (P), Visakhapatnam (V), Chennai (C), Kochi (K), Mormugao (M) and Okha (O) from where tide-gauge data were used in Figure 1. Mormugao is a port located at the mouth of the Zuari estuary.

Figure 3: (a) Depth (m) with respect to mean sea level along a line in the middle of the main

channel of Mandovi. The horizontal scale gives distance (km) from the mouth of the two estuaries. The depth was computed by adding 1.3 m to the depths given in charts published by the Ministry of Shipping and Transport, Government of India. These charts are available only for those parts of the estuarine network used by iron-ore barges. Mean sea level at Mormugao is 1.3 m above Spring Low Water. **(b)**

Cross-sectional area (10^6 m^2), with respect to mean sea level, of the main channels of the Mandovi (re-drawn from Shetye et al., 2007).

Figure 4: Observed water level (cm) during the period of observation. The horizontal axis gives date and month. (Re-drawn based on data presented in Sundar and Shetye, 2005).

Figure 5: Time-series of de-tided (red) and de-tided 2-day low-passed (black) water level in March – April 2003 in the Mandovi estuary at the locations shown in the lower left hand corner of each panel with the distance of the station from mouth shown in brackets. A tick on the time axis shows beginning of the day with the date shown below the tick.

Figure 6: Morlet wavelet power spectra for water level at locations shown in the lower left corner of each panel with distance from the mouth of the estuary given in brackets. The wavelet power is shown in logarithmic scale to the base 2. Wavelet analysis is a tool for analysis of non-stationary time-series data. Wavelet analysis gives the temporal evolution of amplitudes (or phases) of various frequencies in the data. The thick black curve shows the cone of influence (COI). Edge effects due to the finite length of the time-series data are important in the region outside the COI. Note that, on the COI, the Fourier period and the duration of observation are equal (See Torrence and Compo, 1998; and Emery and Thomson, 2001).

Figure 7: Morlet wavelet power spectra for along-shore current measured at the mouth of the Mandovi and Zuari. The thick black curve shows the cone of influence (COI) for the wavelet power spectra. The wavelet power is shown in logarithmic scale to the base 2.

Figure 8: Morlet wavelet power spectra for cross-shore and along-shore wind stress measured near the mouth of the Mandovi and Zuari estuaries. The thick black curve shows the cone of influence (COI) for the wavelet power spectra. The wavelet power is shown in logarithmic scale to the base 2.

Figure 9: Observed along-shore velocity (m s^{-1}) and computed along-shore geostrophic velocity (m s^{-1}) off Mormugao. See Figure 2 for the location of the current meter. Geostrophic velocity is computed using equation (1).

Table A1: Values of wavelength of incident wave, amplification length of incident wave, wavelength of reflected wave and decay length of reflected wave corresponding to the parameters suitable to the Mandovi estuary using the expression for $k_{1,2}$.

Depth (m)	Period (day)	α	Wave length of incident wave (km)	Amplification length of incident wave (km)	Wave length of reflected wave (km)	Decay length of reflected wave (km)
2.0	1/8	6.67856	55.57	15.48	55.57	5.05
2.0	1/4	3.33928	84.54	30.14	84.53	6.01
2.0	1/2	1.66964	137.02	70.19	137.02	6.78
2.0	1	0.83482	242.27	205.48	242.27	7.24
2.0	2	0.41740	460.93	724.96	460.93	7.42
2.0	5	0.16696	1132.86	4341.93	1132.86	7.49
2.0	10	0.08348	2259.89	17255.78	2259.89	7.50
3.0	1/8	4.45237	70.61	22.46	70.61	5.62
3.0	1/4	2.22619	111.05	48.14	111.05	6.49
3.0	1/2	1.11309	189.19	127.97	189.19	7.08
3.0	1	0.55655	350.70	422.77	350.70	7.37
3.0	2	0.27827	683.78	1586.57	683.78	7.46
3.0	5	0.11131	1696.05	9722.54	1696.05	7.49
3.0	10	0.05565	3388.19	38788.27	3388.19	7.50
5.0	1/8	2.67142	97.93	38.67	97.93	6.28
5.0	1/4	1.33571	163.01	96.70	163.01	6.96
5.0	1/2	0.66786	296.18	303.60	296.18	7.32
5.0	1	0.33392	572.09	1112.81	572.09	7.45
5.0	2	0.16696	1132.86	4341.93	1132.86	7.49
5.0	5	0.06679	2823.97	26938.37	2823.97	7.50
5.0	10	0.03339	5645.59	107638.26	5645.59	7.50

Figure 1

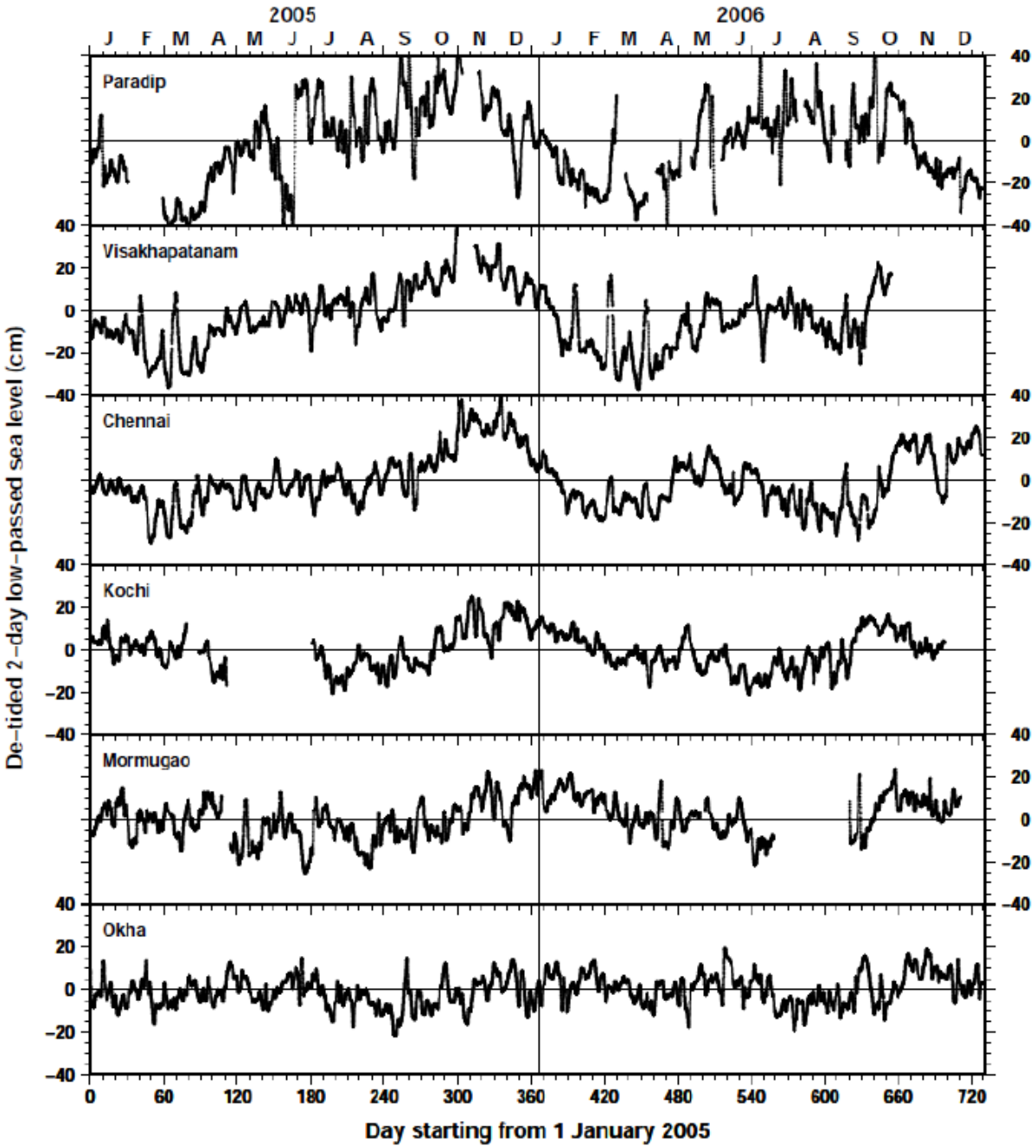
2005
2006
J F M A M J J A S O N D J F M A M J J A S O N D
Paradip
Visakhapatanam
Chennai
Kochi
Mormugao
Okha
De-tided 2-day low-passed sea level (cm)
40
20
0
-20
-40
0 60 120 180 240 300 360 420 480 540 600 660 720
Day starting from 1 January 2005

Figure 2

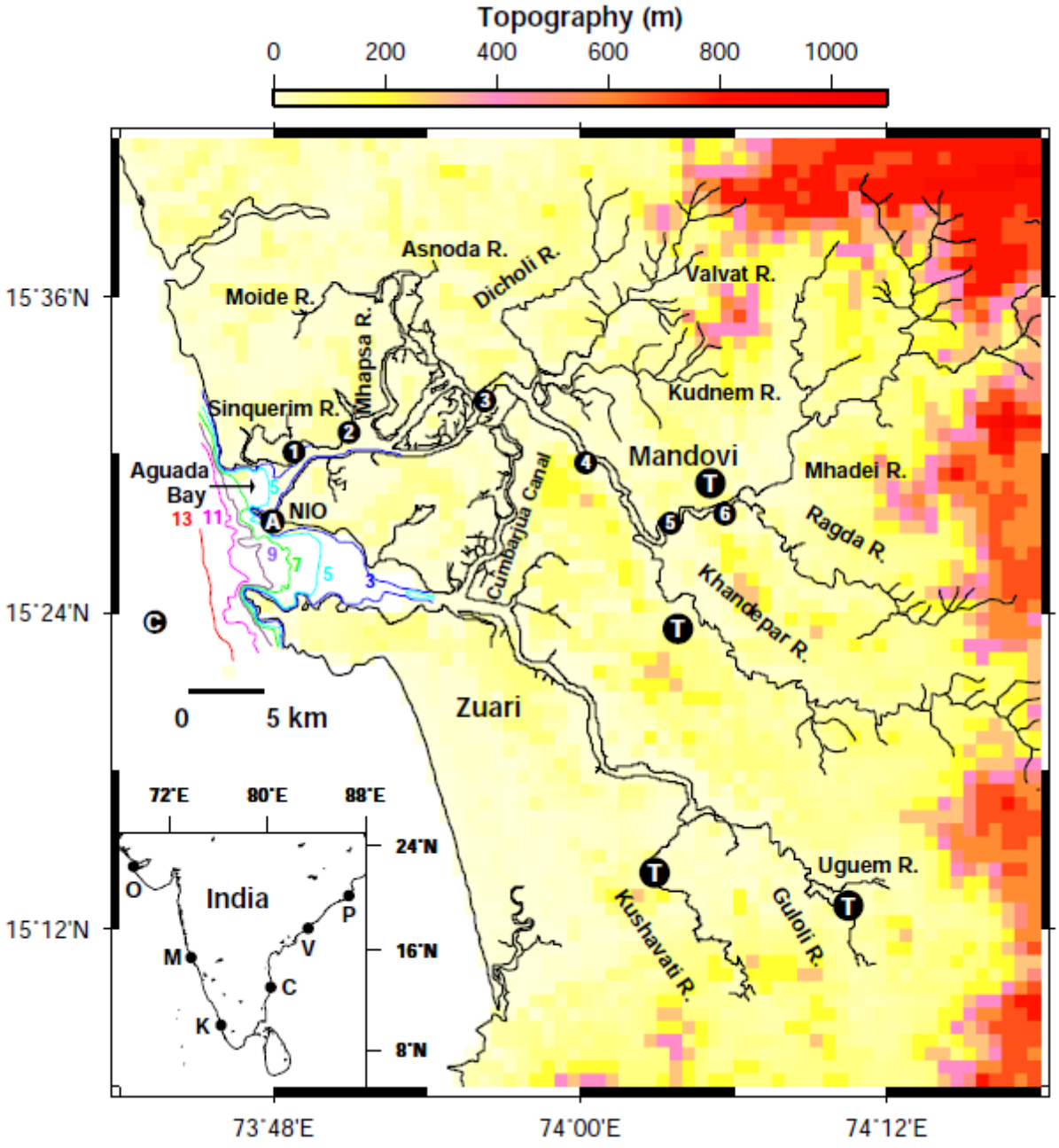
Topography (m)
0
200
400
600
800
1000
Asnoda R.
Dicholi R.
Valvat R.
Moide R.
Mhapsa R.
Kudnem R.
Sinquerim R.
Mandovi
Mhadei R.
Aguada
Bay
NIO
Cumbarjua Canal
Ragda R.
Khandepar R.
Zuari
Uguem R.
Kushavati R.
Guloli R.
India
15°36'N
15°24'N
15°12'N
73°48'E
74°00'E
74°12'E
72°E
80°E
88°E
24°N
16°N
8°N
0
5 km

Figure 3

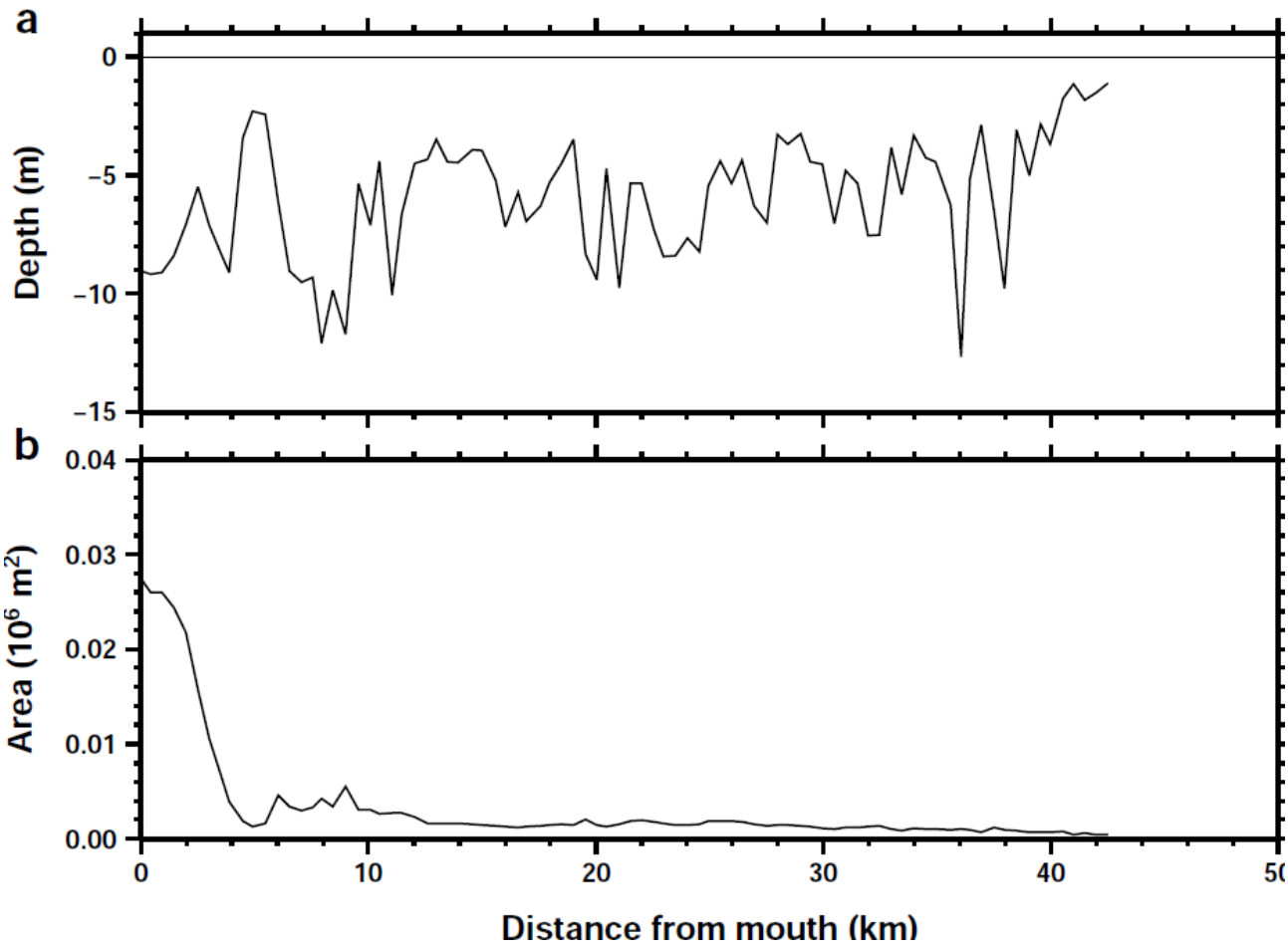
a
0
−5
−10
−15
Depth (m)
b
0.04
0.03
0.02
0.01
0.00
Area (10^6 m^2)
0
10
20
30
40
50
Distance from mouth (km)

Figure 4

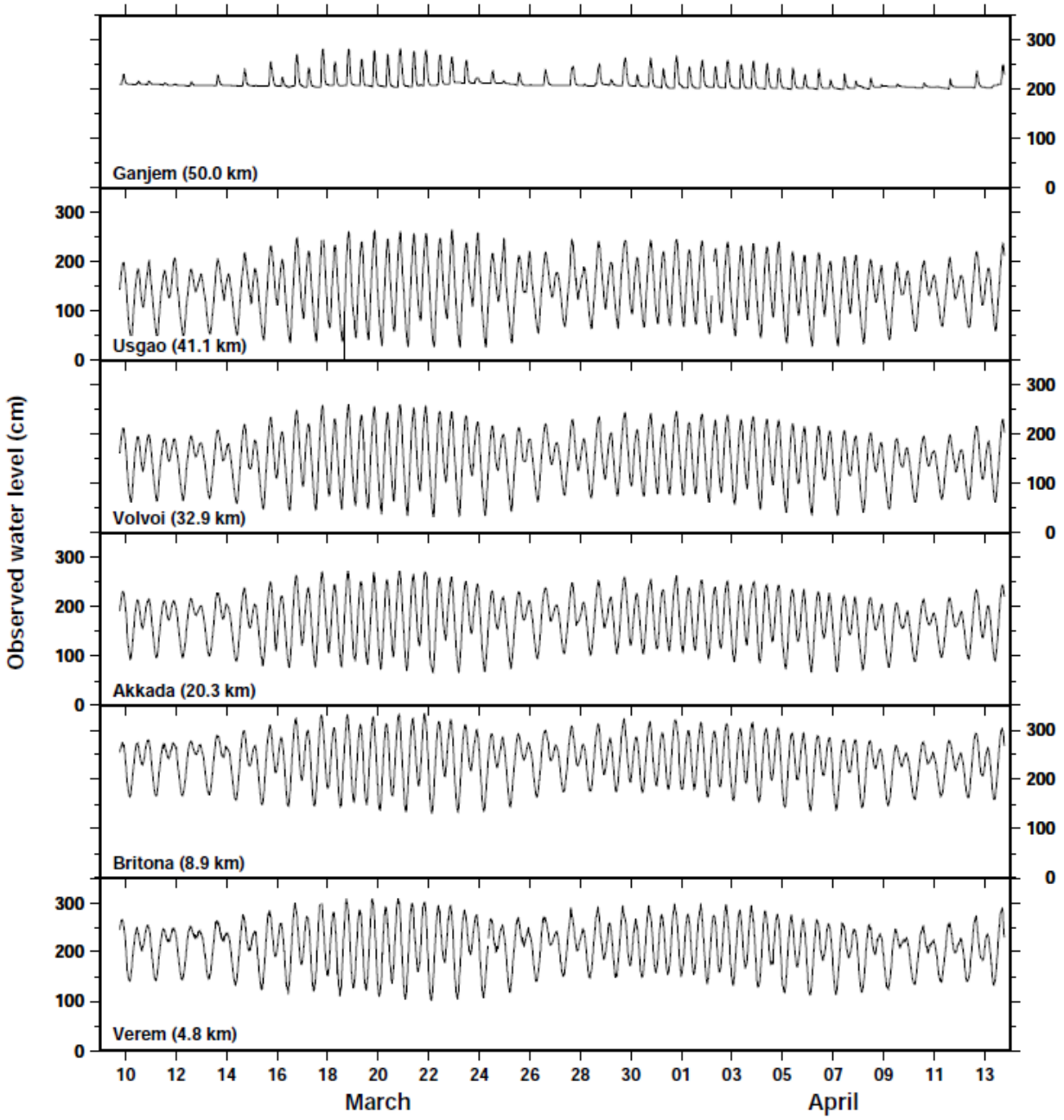
Observed water level (cm)
Ganjem (50.0 km)
Usgao (41.1 km)
Volvoi (32.9 km)
Akkada (20.3 km)
Britona (8.9 km)
Verem (4.8 km)
300
200
100
0
10
12
14
16
18
20
22
24
26
28
30
01
03
05
07
09
11
13
March
April

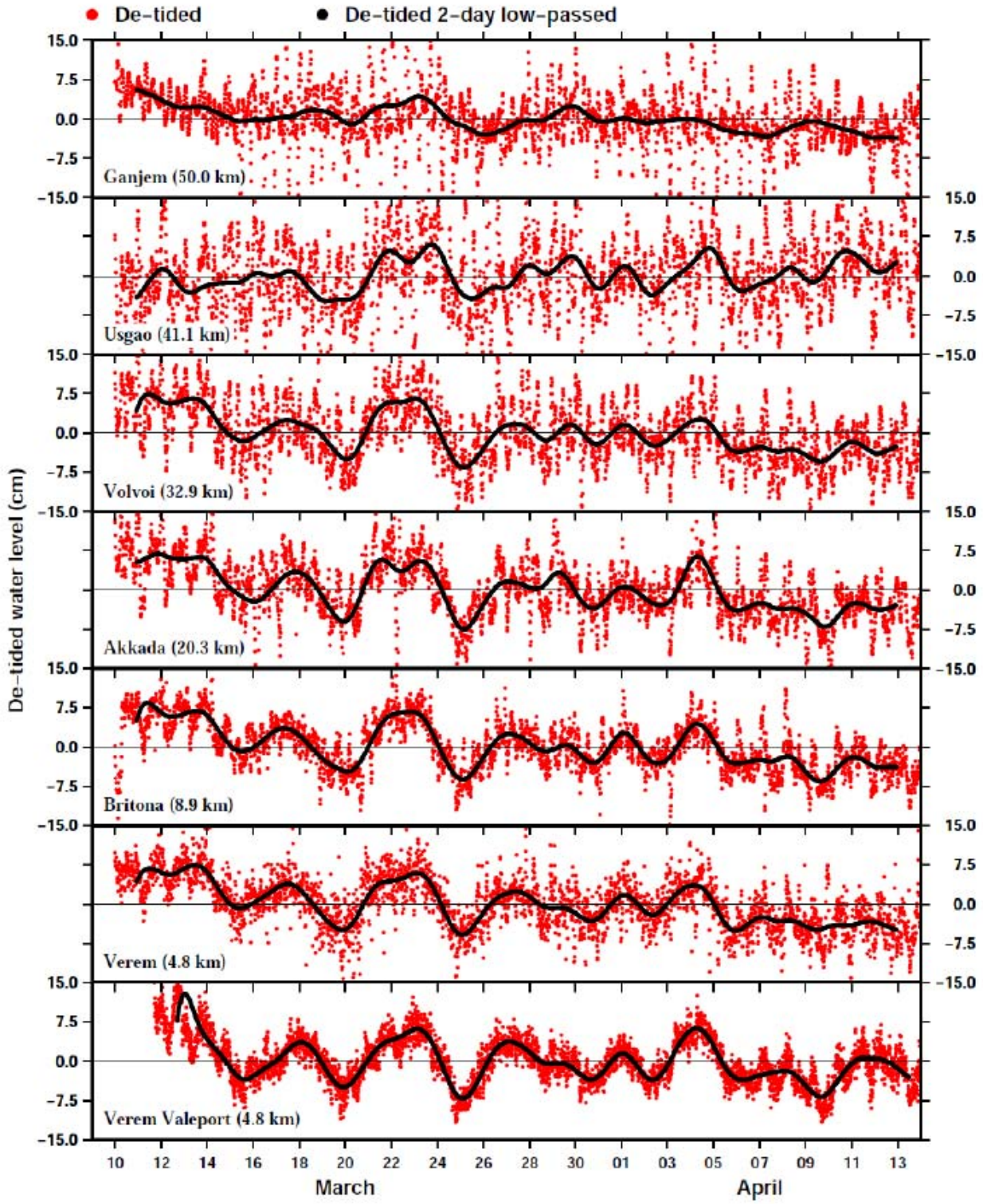
De-tided
De-tided 2-day low-passed
De-tided water level (cm)
Ganjem (50.0 km)
Usgao (41.1 km)
Volvoi (32.9 km)
Akkada (20.3 km)
Britona (8.9 km)
Verem (4.8 km)
Verem Valeport (4.8 km)
15.0
7.5
0.0
-7.5
-15.0
10
12
14
16
18
20
22
24
26
28
30
01
03
05
07
09
11
13
March
April

Figure 5

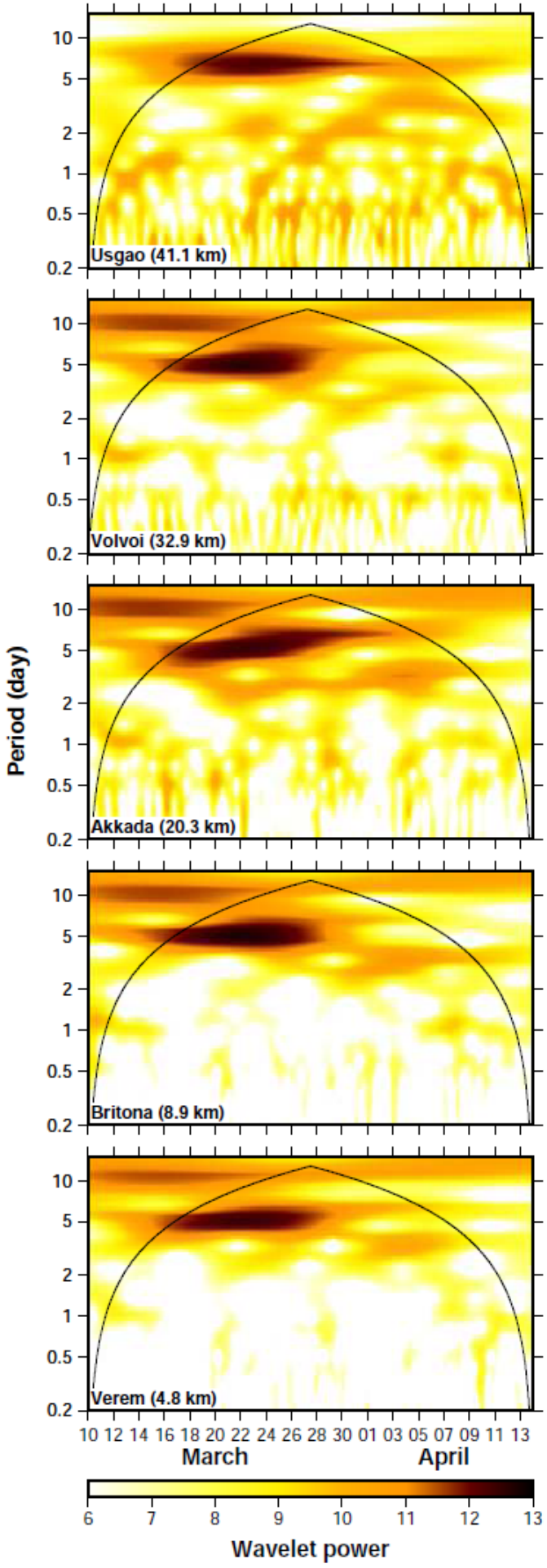
Usgao (41.1 km)
Volvoi (32.9 km)
Akkada (20.3 km)
Britona (8.9 km)
Verem (4.8 km)
Period (day)
10
5
2
1
0.5
0.2
10 12 14 16 18 20 22 24 26 28 30 01 03 05 07 09 11 13
March
April
6 7 8 9 10 11 12 13
Wavelet power

Figure 6

Figure 7

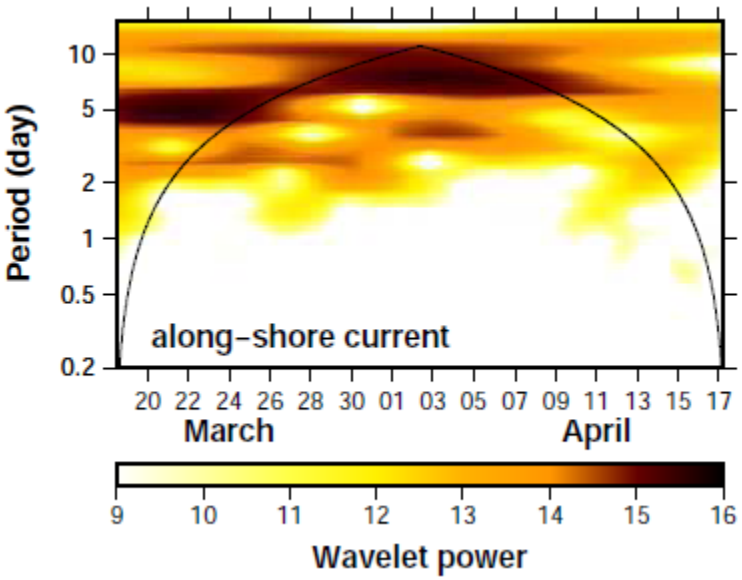
Period (day)
10
5
2
1
0.5
0.2
along−shore current
20 22 24 26 28 30 01 03 05 07 09 11 13 15 17
March
April
9 10 11 12 13 14 15 16
Wavelet power

Figure 8

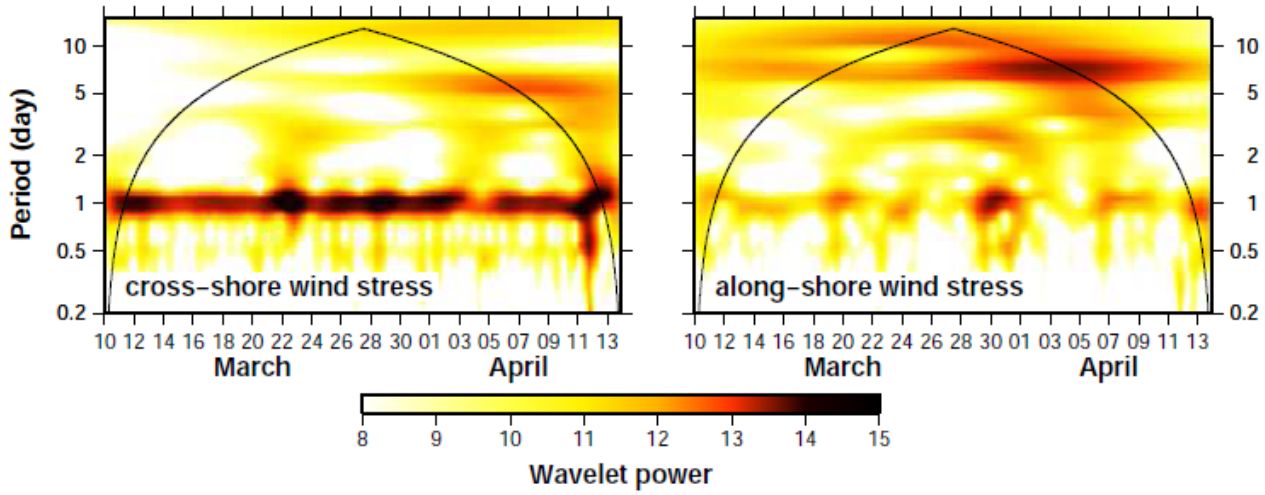

Figure 9